Journal of Drug Delivery Science and Technology 117 (2026) 108020

Contents lists available at ScienceDirect

Journal of Drug Delivery Science and Technology

journal homepage: www.elsevier.com/locate/jddst

Hybrid poly(ε-caprolactone)–carbon dot nanoparticles as self-tracking theranostic tools for precise docetaxel delivery

Roberta Cillari, Francesca Terracina, Sergio Sciré, Nicolò Mauro *, Gennara Cavallaro

Department of "Scienze e Tecnologie Biologiche, Chimiche e Farmaceutiche" (STEBICEF), University of Palermo, Via Archirafi, 32, 90123, Palermo, Italy

ARTICLE INFO

Keywords:
PCL
Carbon nanodots
Breast cancer
Docetaxel
Theranostics
Precision cancer therapy

ABSTRACT

Hybrid nanocomposites combining biodegradable polymers with fluorescent nanomaterials offer innovative strategies for theranostic applications. In this work, carbon nanodots (CDs) were successfully incorporated into a polycaprolactone (PCL) matrix to create a hybrid material exhibiting intrinsic multicolor fluorescence and high potential for sustained image-guided anticancer drug release. The resulting PCL–CDs blend was used to fabricate self-tracking biodegradable nanoparticles (NPs) through a green nanoprecipitation process optimized for sustained drug delivery. When loaded with docetaxel (DTX), used as a model hydrophobic drug, the PCL–CDs NPs achieved a high drug-loading capacity (~16.5 %) and an encapsulation efficiency of 98 %, while maintaining an average particle size of approximately 200 nm. The NPs exhibited a sustained, pH-responsive release profile and demonstrated significant cytotoxic activity in a triple-negative breast cancer model. Furthermore, the formulation showed excellent colloidal stability in aqueous dispersion for up to 10 days, guaranteeing suitable storage before the administration. We also studied the best cryoprotection strategy to prepare a stable lyophilized powder for long-lasting storage of the PCL-CDs@DTX NPs, identifying L-arginine as the best option to obtain redispersible systems with an appropriate diameter (~200 nm). By integrating fluorescence-based bioimaging with controlled chemotherapeutic delivery, these PCL–CDs NPs represent a robust, versatile, and sustainable theranostic nanoplatform with strong potential for precision cancer therapy.

1. Introduction

Carbon nanodots (CDs) have emerged as highly versatile nanomaterials, offering huge potential in many biomedical and pharmaceutical applications such as in cancer theranostics [1–3]. CDs enable cancer theranostics by integrating fluorescence imaging and targeted therapy within a single platform, allowing real-time disease monitoring and image-guided personalized treatment. CDs are readily obtainable by straightforward, low-cost methods and exhibit unique features, including tunable multicolor fluorescence, which offers appealing opportunities for imaging and sensing of biological tissues [4,5]. Owing to their high water and physiological fluid dispersibility, low toxicity, and excellent biocompatibility, CDs are particularly well suited for biomedical applications [6–8]. In addition to their use as stand-alone nanosystems, CDs may be incorporated into polymer matrices to obtain nanocomposites with tailored properties and functions, depending on the nature of the polymer and the selected embedding strategy [9]. Even though there are other nanoparticles with comparable theranostic potential (e.g., magnetic nanoparticles [1], gold nanoparticles [2], silver nanoparticles [3,4], and carbon nanotubes [5]), CDs are ultrasmall (d < 10 nm) and can efficiently diffuse across multiple biological barriers to be also bio-eliminated through both renal clearance and hepatic pathways [6].

When used as nanofillers in biopolymer matrices, CDs reinforce the mechanical characteristics of the polymer and provide self-tracking properties [10]. This combination yields hybrid biomaterials ideal for preparing hydrogels and scaffolds for tissue engineering [11,12], wound dressing [13], biosensing [14], and drug delivery [15]. However, the incorporation of CDs into core-shell nanosystems such as nanoparticles and micelles requires tedious and expensive surface hydrophobization procedures, which preclude real-world applications [7].

Hybrid nanocomposites based on polyesters, which are well-recognized FDA-approved biopolymers, are advantageous for biomedical use due to their superior biodegradability and low toxicity [16]. Polyesters undergo hydrolysis and enzymatic degradation *in vivo*, ensuring complete elimination with the release of non-toxic by-products [17]. Furthermore, the hydrophobic nature of polyesters facilitates the encapsulation and sustained release of poorly water-soluble drugs, such

* Corresponding author.
E-mail address: nicolo.mauro@unipa.it (N. Mauro).

https://doi.org/10.1016/j.jddst.2026.108020
Received 5 November 2025; Received in revised form 8 January 2026; Accepted 13 January 2026
Available online 13 January 2026

as chemotherapeutic agents, enhancing their localized delivery to target tissues [18]. Although poly(caprolactone) (PCL) is less frequently employed than polylactic acid (PLA) or polylactic-co-glycolic acid (PLGA) polyester for producing drug delivery nanosystems [19], PCL is an attractive candidate for nanocomposites fabrication when long-term controlled drug delivery is required [20,21]. However, PCL nanoparticles lack intrinsic fluorescence or imaging contrast, necessitating labeling with contrast agents for *in vitro/in vivo* real-time monitoring of their distribution [22,23]. While the inclusion of organic emissive dyes in PCL nanoparticles is a common approach for imparting traceability, CDs surpass traditional dyes in terms of optical stability, resistance to photobleaching, and cytocompatibility, offering significant advantages for bioimaging and biosensing [24,25]. Notwithstanding the high optical performance of CDs in solution, they typically undergo fluorescence quenching phenomena when in solid state. Reaching solid state emissive CDs such as in nanoparticles is not trivial and demands surface functionalization to both compatibilize CDs with the polymer matrix and avoid dot-to-dot interactions responsible for quenching [8–10].

Herein, PCL–CDs blends were produced for the first time via a green, one-pot melt-mixing process, without the use of solvents or additional chemicals, while preserving both the long-term degradability of PCL and the photoluminescent properties of the carbon dots. The PCL–CDs blends were subsequently employed to prepare stable nanoparticles through a simple and scalable nanoprecipitation method for the delivery of the antitumor drug docetaxel (DTX), thereby proposing their application in the treatment of triple-negative breast cancer (TBNC).

2. Materials and methods

2.1. Materials

Polycaprolactone (PCL) (Mn 80,000 Da, PD 1.89), L-arginine (99.5 %), mannitol (99 %), poly (ethylene glycol) (Mw 4 kDa), docetaxel (DTX, Ph. Eur.), acetone (99.9 %), and dichloromethane (DCM, 99.9 %) were purchased from Merck (Italy). Human triple-negative breast cancer cells (MDA-MB-231) were obtained from "Istituto Zooprofilattico Sperimentale della Lombardia e dell'Emilia Romagna".

2.2. Methods

Dynamic light scattering (DLS) measurements were performed using a Malvern Zetasizer Nano ZS (Rome, Italy) equipped with a 532 nm laser operating at fixed scattering angle (173°).

Zeta-potential was evaluated by aqueous electrophoresis measurements, using the same apparatus. The Zeta-potential values (mV) were calculated from electrophoretic mobility using the Smoluchowski relationship.

All analyses were performed on three different samples and results are expressed as mean values ± standard deviation (n = 3 samples, n = 6 measurements per sample).

Scanning transmission electron microscopy (STEM) analysis was performed using a FEI Tecnai G2 200 kV S -TWIN microscope equipped with a 4 K camera (Thermo Fisher Scientific). Samples were prepared by drop deposition (20 μL of 0.1 mg mL^{-1} water solution) on a 200-mesh copper grid coated with carbon black film and left to dry.

2.3. Incorporation of carbon nanodots in a polycaprolactone matrix

Carbon nanodots (CDs), synthesized as previously reported [26], were dispersed in a water-acetone (1:2) mixture and sonicated for 1 h. Then, a PCL solution in DCM was added, and the mixture was strongly agitated to obtain an emulsion of the immiscible solvents. The mixture was dried under vacuum and physically mixed with PCL pellets. The solid mixture was melted by heating (160 °C), and a mechanical stress was applied to favor a homogeneous incorporation of CDs within the polymeric mass. After 6 h, the obtained PCL-CDs blend was cooled to room temperature and recovered at the solid state. The procedure was performed using 15 g of PCL and increasing amounts of CDs (15, 37.5, 75, 105, 150, and 225 mg), corresponding to 0.1, 0.25, 0.5, 0.7, 1.0, and 1.5 % w/w.

2.4. Characterization of the PCL-CDs blend

The morphology of PCL-CDs blends was investigated by widefield fluorescence microscopy, using an Axio Cam MRm (Zeiss). Micrographs were acquired at 5× magnification and the exposure time was fixed at 30 ms for DAPI channel, 60 ms for FITC channel, and 300 ms for TexasRed Channel.

2.5. Preparation of PCL-CDs nanoparticles

PCL-CDs blends were solubilized in acetone (5 mg, 10 mL) under sonication (3 × 5 min). Then, 2 mL of water was added all at once under stirring to induce nanoprecipitation. The samples were concentrated by rotary evaporation (100 - 50 mbar) while adding up to 4 mL of water, and until the complete evaporation of acetone. PCL-CDs were therefore obtained as aqueous dispersions.

2.6. Incorporation of docetaxel within PCL-CDs NPs

PCL-CDs blends (5 mg) and docetaxel (DTX, 1 mg) were solubilized in 10 mL of acetone under sonication. Then 2 mL of water were added all at once under stirring to induce nanoprecipitation. The samples were concentrated by rotary evaporation while adding up to 4 mL of water and until the complete evaporation of acetone. The obtained aqueous dispersions of docetaxel-loaded PCL-CDs NPs, indicated as PCL-CDs@DTX, were filtered through a 1.2 μm syringe filter to remove unloaded free drug.

The amount of DTX incorporated within PCL-CDs@DTX was evaluated by HPLC analysis. Briefly, PCL-CDs@DTX (1 mg mL^{-1}) were freeze-dried and reconstituted in the HPLC mobile phase, consisting of a water/acetonitrile (45:55) mixture. Samples were filtered through a 0.22 μm RC syringe filter and analyzed by HPLC, using an Agilent 1260 Infinity II instrument equipped with a Quaternary Pump VL G7111A and a VWD detector G7114A, 20 μL injector, and a computer integrating apparatus (OpenLAB CDS ChemStation Workstation). The analysis was conducted using a reversed-phase Luna Phenomenex C18 column with a 1.0 mL min^{-1} flow rate. The UV detector was fixed at 230 ± 4 nm. A calibration curve of DTX (0.01–0.1 mg mL^{-1})($y = 22114x$, $R = 0.999$) was used for quantitative calculations.

To evaluate the release of DTX, PCL-CDs@DTX nanoparticles (1.5 mg mL^{-1}, 5 mL) were placed in a dialysis tube (2 kDa MWCO), and immersed in 15 mL of PBS pH 7.4 (0.1 % w/v Tween 80) or acetate buffer pH 5.5 (0.1 % w/v Tween 80). At scheduled time intervals (0.5, 2, 4, 8, 24, and 48 h) an aliquot of the external phase was withdrawn (0.225 mL) and replaced with fresh medium. Sampled aliquots were diluted with acetonitrile (0.275 mL), centrifuged (9000 rpm, 9 min), and analyzed by HPLC using the same method employed for drug loading evaluation.

2.7. Evaluation of PCL-CDs NPs biological properties

The internalization of PCL-CDs NPs by MDA-MB-231 cells was evaluated by widefield fluorescence microscopy. Cells were seeded at 5.0 × 103 cells per well in a 8-well Nunc Lab-Tek chambered coverglass (Thermo Fisher Scientific), and cultured for 24 h. Then, the culture medium was replaced with PCL-CDs (0.25 %), PCL-CDs (0.5 %) or PCL-CDs(0.7 %) dispersions in DMEM (200 μL, 0.5 mg mL^{-1}). At scheduled time intervals (24 h, 48 h), the nanoparticles' dispersion was removed and cells were washed twice with PBS, before fixing with 4 % buffered formaldehyde. Micrographs were acquired using an Axio Cam MRm (Zeiss) widefield fluorescence microscope operating at 100×

magnification.

A preliminary evaluation of PCL-CDs and PCL-CDs@DTX cytotoxic effect was performed on MDA-MB-231 cells. Cells were seeded at 7.5 × 103 cells per well and cultured for 24 h. The culture medium was then replaced with DTX solutions in DMEM (20-1.25 μ g mL^{-1}, 0.15 mL), or PCL-CDs@DTX, and PCL-CDs NPs dispersions at equivalent drug concentration. After 48 h, the treatment was removed, and cells were washed with DPBS before performing the MTS cell viability test (CellTiter 96® AQueous assay - Promega). Data were reported as percentage cell viability assuming control cells as 100 % cell viability. The analysis was performed at least in triplicate.

2.8. Study of PCL-CDs@DTX stability after freeze-drying

Cryoprotectant including PEG 4 kDa, mannitol, and L-arginine were added to PCL-CDs@DTX in water dispersion (1 mg mL^{-1}) at 5 % w/v concentration. The mixtures were freeze-dryed, and subsequently ultrapure water was added to resuspend the powders. Dynamic light scattering (DLS) measurements were performed before and after freeze-drying the mixtures.

2.9. Statistical analysis

The statistical significance of repeated datasets was evaluated by ANOVA one-way analysis of variance, followed by Tukey's post-hoc test for single pair comparisons, performed using the GraphPad Prism software. Data were reported as mean value ± standard deviation (n = 6). Comparisons were considered statistically significant at $p < 0.05$ (*), $p < 0.01$ (**), and $p < 0.001$ (***).

3. Results and discussion

3.1. Development of a composite material by physical blending of carbon nanodots in a PCL matrix

The incorporation of carbon nanodots (CDs) within a PCL polymeric matrix was achieved by dispersing the nanoparticles in molten PCL under mechanical stress, imposed using an Archimedean screw. The procedure was repeated using increasing amounts of CDs (0.1, 0.25, 0.5, 0.7, 1.0, 1.5 % w w^{-1}) to obtain 6 different samples with different compositions. After cooling, the resulting PCL-CDs blends were obtained as solid polymeric pellets, which were subsequently chopped into smaller pieces to facilitate their further processability (Fig. 1).

The morphological composition of the blends was investigated by widefield fluorescence microscopy, leveraging the inherent photoluminescence of CDs. As shown in Fig. 2, PCL-CDs composites present strong multicolor fluorescence emission that enables obtaining clear fluorescence microscopy micrographs in the DAPI blue (Fig. 2a–aV), FITC (Fig. 2b–bV), and Texas Red (Fig. 2c–cV) channels, corresponding to blue, green, and red fluorescence, respectively. The self-fluorescence of the composite material in the red region is particularly interesting for biomedical purposes, as it provides self-tracking potential within the biological transparency window, offering appealing opportunities for *in vivo* imaging. The uniform distribution of the optical emission indicates that CDs are homogeneously dispersed throughout the polymeric matrices, with only a few dark spots attributable to fluorescence quenching due to interparticular interactions, observable with increasing CD concentration.

3.2. Preparation of PCL-CDs nanoparticles by nanoprecipitation

The PCL-CDs blends prepared were used to obtain nanoparticles by rapid solvent displacement, using acetone as green dispersant and water as precipitation solvent. Compared to other organic solvents commonly used to dissolve hydrophobic polyesters, acetone was preferred due to its lower environmental impact, with the aim of ensuring the sustainability of the productive process in view of its potential industrial scalability [27]. Acetone is indeed classified as a low-toxicity, class 3 solvent by the FDA and has received favorable sustainability ratings in several solvent assessment frameworks [6]. Despite several attempts, the nanoprecipitation of PCL-CDs blends with higher concentrations of CDs was unsuccessful due to the rapid destabilization of the obtained nanoparticles in the aqueous phase. Instead, the nanoprecipitation of PCL-CDs(0.1 %), PCL-CDs(0.25 %), PCL-CDs(0.5 %), and PCL-CDs(0.7 %) successfully produced nanoparticles with desirable properties for biomedical applications (Table 1). In particular, all the obtained nanoparticles (PCL-CDs NPs) presented a Z-average below 200 nm, falling within the optimal size range for preferential uptake by cancerous target tissues by enhanced permeability and retention (EPR) effect [28,29]. The size distribution of the nanoparticles was extremely narrow, with a polydispersity index of <0.2 nm, supporting the good homogeneity of the nanoparticles as aqueous dispersion. The strongly negative Z-potential of the samples, probably due to the disposition of carboxylic groups of CDs at the PCL/water interface, favors the colloidal stability of PCL-CDs NPs, providing an adequate electrostatic repulsion between the nanoparticles, thereby preventing aggregation or flocculation phenomena [30].

The morphology of PCL-CDs NPs was investigated by scanning transmission electron microscopy (STEM) analysis. As shown in Fig. 3, STEM micrographs showed elongated ellipsoidal objects with dimensions consistent with those calculated by DLS analysis. Interestingly, the NPs exhibited a darker core surrounded by a lighter homogeneous

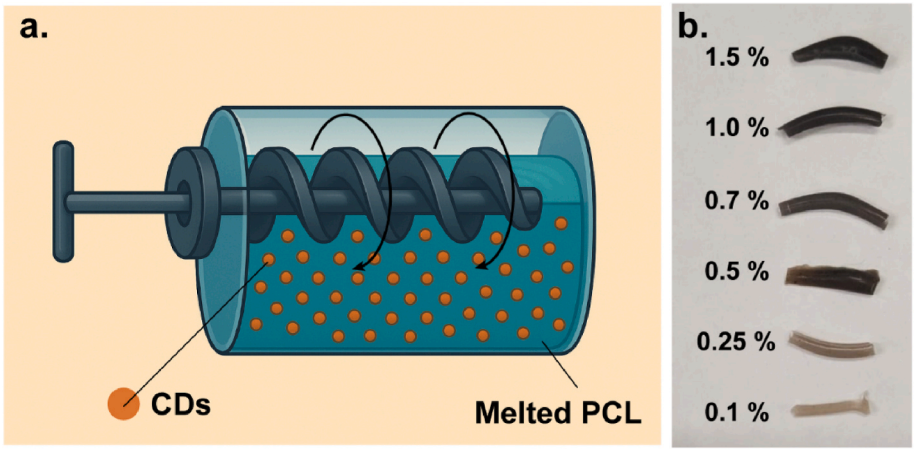

Fig. 1. Preparation of PCL-CDs blends. Illustration of the preparation process (a) and photographs of PCL-CDs blends at increasing CDs concentration (b).

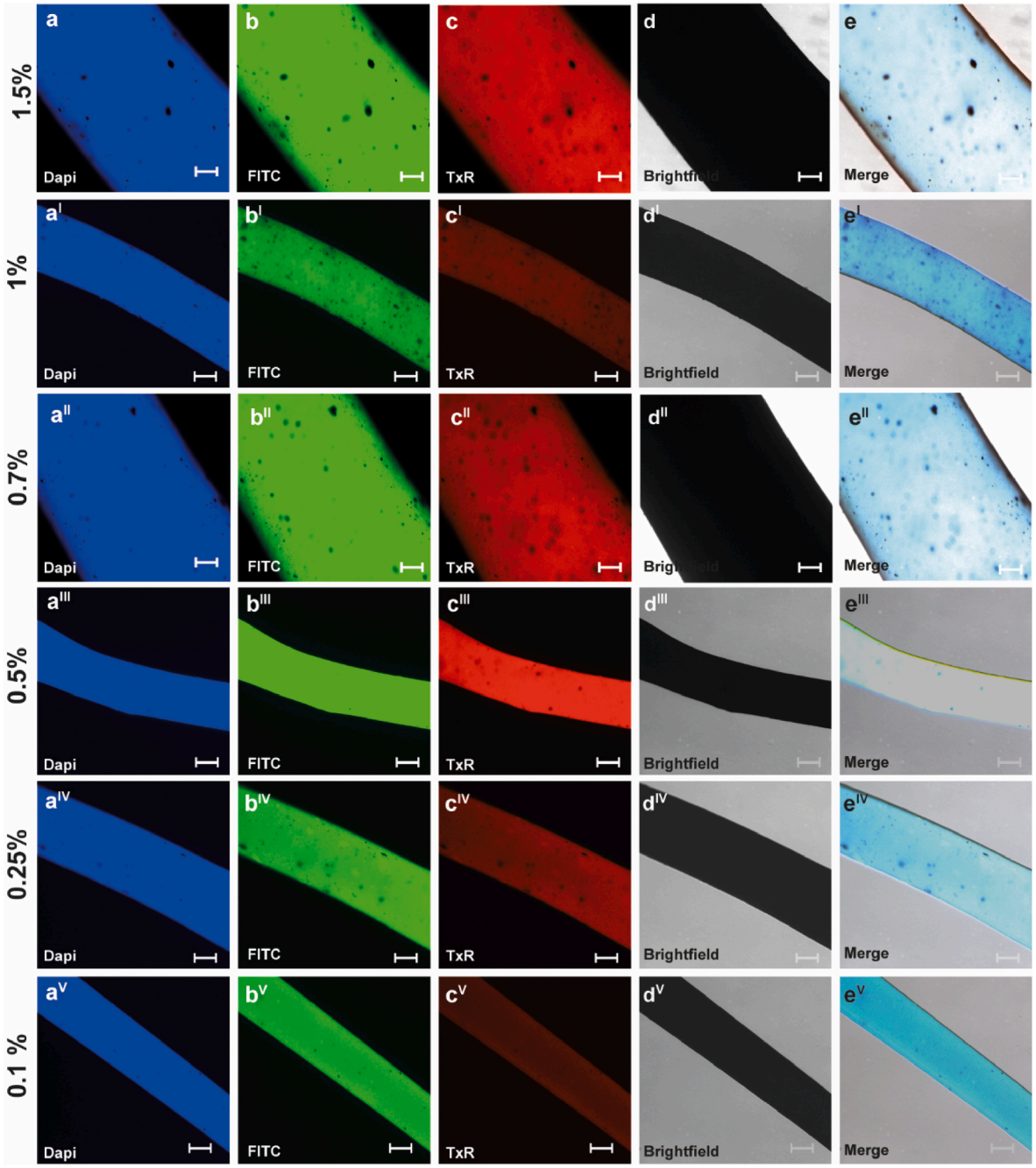

Fig. 2. Optical and morphological features of PCL-CDs blends. Micrographs of PCL-CDs blends (0.1–1.5 % CDs) acquired by widefield optical microscopy in the DAPI (a-aV), FITC (b-bV), TexasRed (c-cV) channels, and brightfield (d-dV) channels, and merge images (e-eV) (Magnification: 5×; Scalebar: 200 μm).

Table 1
Characterization of PCL-CDs NPs.

Sample	Z-average (nm)	PDI	Z-potential (mV)[a]
PCL-CDs(1.5 %) NPs	/	/	/
PCL-CDs(1.0 %) NPs	/	/	/
PCL-CDs(0.7 %) NPs	192.0 ± 10.8	0.069	−38.3 ± 0.7
PCL-CDs(0.5 %) NPs	178.3 ± 9.4	0.035	−37.3 ± 0.2
PCL-CDs(0.25 %) NPs	172.0 ± 5.4	0.054	−36.5 ± 0.6
PCL-CDs(0.1 %) NPs	190.1 ± 7.2	0.040	−36.5 ± 0.6

Mean size, PDI values, and Z-potential of PCL-CDs nanoparticles. Data are reported as mean value ± SD (n = 3).

[a] Conductivity lower than 1 mS cm^{-1}

shell-like structure, suggesting an ordered arrangement of the elements of the PCL-CDs blend during nanoprecipitation, with CDs located in the NPs core and PCL exposed on the outer surface.

3.3. Incorporation of docetaxel in PCL-CDs nanoparticles

The nanoprecipitation protocol was repeated in the presence of docetaxel (DTX) to incorporate the drug within PCL-CDs NPs during their formation. Due to the highly hydrophobic nature of the drug, it was solubilized in the acetone dispersion of PCL-CDs blends before precipitating via solvent displacement with water. The incorporation of DTX resulted in an alteration of the average hydrodynamic diameter and of the Z-potential of the NPs. In particular, PCL-CDs(0.7 %)@DTX exhibited the highest size, reaching ~ 230 nm, while maintaining Z-potential

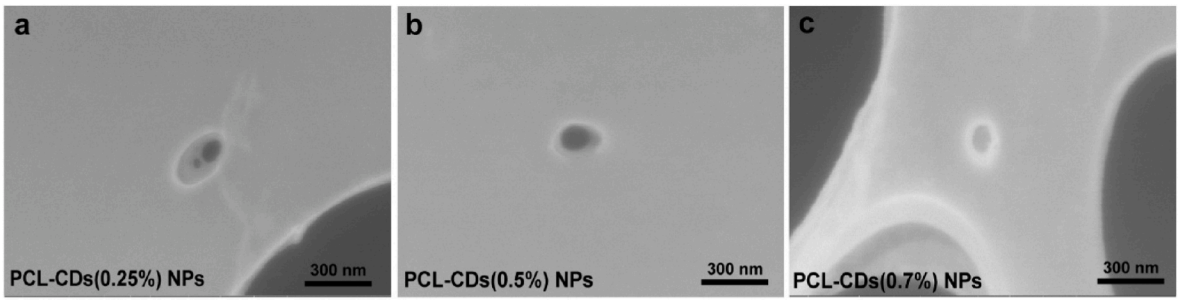

Fig. 3. STEM micrographs of isolated PCL-CDs nanoparticles; Micrographs of PCL-CDs(0.25 %) NPs (a), PCL-CDs(0.5 %) NPs (b), and PCL-CDs(0.7 %) NPs (c). Scalebar: 300 nm.

values comparable to those of unloaded nanoparticles, suggesting a preferential drug incorporation within the nanoparticle core with minimal surface interactions (Table 2). Conversely, PCL-CDs(0.1 %)@DTX displayed a smaller Z-average and a significantly higher Z-potential compared to unloaded NPs, indicating the presence of surface interactions with DTX. Intermediate behavior was observed for the other samples, as PCL-CDs(0.5 %)@DTX and PCL-CDs(0.25 %)@DTX both showed a slight increase in hydrodynamic diameter along with higher Z-potential values, supporting a distributed localization of the drug at both nanoparticles' surfaces and cores.

Table amount of DTX encapsulated in PCL-CDs@DTX NPs was evaluated by HPLC analysis, calculating drug loading (DL) and encapsulation efficiency (EE). Coherently with DLS analysis, PCL-CDs(0.5 %)@DTX and PCL-CDs(0.25 %)@DTX showed the highest DL values (16.51 ± 0.19 % and 14.74 ± 1.6 %) and EE values (98.8 ± 1.18 % and 91.28 ± 9.5 %, respectively), emerging as most promising formulatios. PCL-CDs(0.7 %)@DTX also exhibited a good DL (14.49 ± 0.59), with a slightly lower, but however more than satisfactory EE (86.77 ± 3.56). In contrast, drug loading into PCL-CDs(0.1 %) NPs was less efficient, with a DL remaining below 10 % (EE 56.92 ± 4.29 %). Based on these results, PCL-CDs(0.1 %)@DTX were excluded from further characterization, which focused on the most promising samples. With calculated drug loadings between 149 μg mg^{-1} and 165 μg mg^{-1}, PCL-CDs@DTX demonstrated a superior capacity to encapsulate high amounts of DTX compared to most nanosystems proposed in the literature for DTX delivery, which commonly show a DL lower than 10 % [31,32]. The high loading capacity of PCL-CD nanoparticles can be attributed to the chemical affinity between the drug and the polymer matrix. The hydrophobic nature of PCL facilitates interaction with hydrophobic drugs such as DTX, promoting their incorporation into nanoparticles during nanoprecipitation through affinity loss with the solvent. Using PCL-CDs NPs for DTX delivery enables the potential administration of high drug doses directly dispersed in aqueous media, without resorting to the use of surfactants or other solvents. This represents an advantage of the proposed formulation over Taxotere®, the DTX formulation currently approved for clinical use, which is supplied as a dispersion of the drug in polysorbate 80 and requires a 1 h intravenous infusion for administration after being diluted in a 13 % ethanol solution in water [33].

The composite structure of PCL-CDs@DTX was also designed to provide a gradual release of the drug payload, ensuring that a therapeutic dose is achieved at the target site through prolonged release and avoiding off-target cytotoxic effects. Considering the typical slow degradability of polyesters in aqueous media [17], PCL-CD@DTX are expected to remain stable in the short term, with minimal DTX release. The destabilization of the nanoparticles, and the subsequent release of docetaxel, are expected to be more pronounced under acidic environments and in the presence of esterases. This effect arises from the accelerated erosion of the PCL–CD matrix through acid- and enzyme-catalyzed hydrolysis of ester bonds [34]]. Therefore, the acidic pH of the tumor microenvironment (TME) and of intracellular compartments, such as lysosomes and endosomes, may function as an internal stimulus to accelerate the erosion of the polymeric matrix, gaining accelerated release of the drug at the target site [17,35]. To assess the pH-dependent DTX release from drug-loaded nanoparticles, we performed release kinetics experiments in buffer solutions at physiological (pH 7.4) and acidic (pH 5.5) conditions. All samples demonstrated a high stability, releasing less than 10 % of drug payload after 48 h (Fig. 4). At physiological pH values, the low release observed could be attributed to the desorption of drug molecules interacting with the surface of the nanoparticle rather than to degradation of PCL. All formulations exhibited an initial burst release followed by a plateau, except for PCL–CDs (0.7 %)@DTX, which showed a slightly higher cumulative release. This behavior can be ascribed to interfacial effects arising from the incorporation of CDs within the polymer matrix (Fig. 3). The presence of polar and acidic surface groups on the CDs likely enhanced local water uptake and created mildly acidic microenvironments at the polymer–water interface, thereby promoting limited hydrolytic degradation of the PCL matrix and facilitating docetaxel diffusion. Nevertheless, this effect remained moderate, indicating that CDs incorporation did not significantly compromise the overall stability of the nanoparticles under physiological conditions.

The expected accelerated release of DTX in acidic conditions was demonstrated for PCL-CDs(0.5 %)@DTX, which released ~ 7 % of the payload at pH 5.5 and only ~ 4 % in physiological conditions after 48h. PCL-CDs(0.7 %)@DTX also exhibited a slightly faster release of DTX in the acidic environment, although the difference was less pronounced since the release at pH 5.5 and pH 7.4 differed by only about 1 %. The observed moderate pH-dependet release behavior of these samples is consistent with drug encapsulation within the polymeric nanoparticle matrix, whose acid-responsive erosion promotes gradual and sustained

Table 2
Characterization of docetaxel-loaded PCL-CDs NPs.

Sample	Z-average (nm)	PDI	Z-potential[a] (mV)	DL (%)	EE (%)
PCL-CDs(0.7 %)@DTX	218.6 ± 8.3	0.020	−35.9 ± 0.5	14.49 ± 0.59	86.77 ± 3.56
PCL-CDs(0.5 %)@DTX	157.6 ± 8.9	0.032	−49.2 ± 2.3	16.51 ± 0.19	98.80 ± 1.18
PCL-CDs(0.25 %)@DTX	176.6 ± 8.9	0.047	−41.0 ± 0.1	14.74 ± 1.60	91.28 ± 9.50
PCL-CDs(0.1 %)@DTX	171.1 ± 9.4	0.055	−41.1 ± 1.1	9.24 ± 0.68	56.92 ± 4.29

Mean size, PDI values, Z-potential of PCL-CDs nanoparticles, drug loading (DL, %), and encapsulation efficiency (EE, %). All data are reported as mean value ± SD (n = 3 samples, n = 6 measurements per sample).
[a] Conductivity lower than 1 mS cm^{-1}

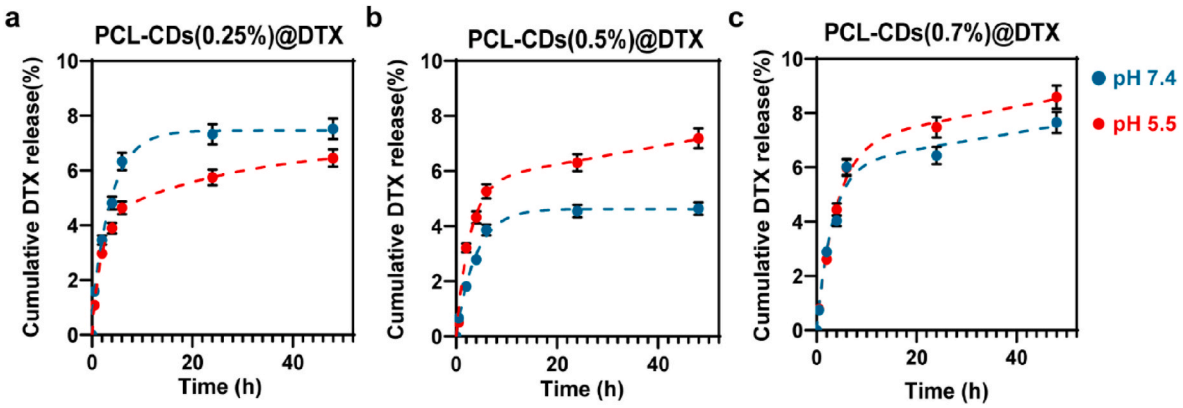

Fig. 4. Evaluation of docetaxel release from PCL-CDs@DTX. Kinetics of DTX release from PCL-CDs(0.25 %)@DTX, PCL-CDs(0.5 %)@DTX, and PCL-CDs(0.7 %)@DTX, in phosphate buffered saline pH 7.4 (blue) and acetate buffer pH 5.5 (red). Mean S.D. N = 3. (For interpretation of the references to color in this figure legend, the reader is referred to the Web version of this article.)

drug release. The biphasic drug release observed, that is initial burst followed by sustained release, in agreement with previous works, could support the hypothesis of a potential EPR-based targeted and long-term drug delivery in solid tumors such as breast cancers [36,37]. Given the high drug loading (14.5 %), the slow and sustained release profile is expected to maintain therapeutically relevant concentrations of DTX in situ following nanoparticle accumulation.

Different considerations must be taken into account for PCL-CDs (0.25 %)@DTX, which showed a higher cumulative release percentage at pH 7.4 than at pH 5.5. This difference is associated with different release curve trends, showing a plateau under physiological conditions and a growing curve under acidic conditions. Several factors may have contributed to this finding, including a heterogeneous distribution of the drug within PCL-CDs(0.25 %)@DTX and a different organization of the polymeric network, which could limit solvent diffusion and polymer erosion at pH 5.5. Moreover, the confinement of CDs in the NPs cores, as shown by STEM micrographs, suggests the isolation of hydrophilic domains within the nanocomposite, reducing favorable interactions with the buffer medium and, consequently, hindering drug release under acidic conditions.

3.4. *Evaluation of the biological properties of PCL-CDs and PCL-CDs@DTX*

The intrinsic fluorescence of the PCL-CDs nanoparticles (PCL-CDs NPs) was exploited to track their cellular uptake by TNBC cells (MDA-MB-231). As shown in Fig. 5, PCL-CDs NPs can be visualized in living cells across the entire visible spectrum (blue to red) using a common fluorescence imaging technique. This suggest a good and versatile theranostic potential of PCL-CDs. Indeed, at least in principle, they could be tracked in living tissues in order to assess a proper localization of the drug payload.

On the other hand, Fig. 5 showed that PCL-CDs NPs were efficiently internalized by cancer cells and distributed throughout the cytoplasm, with no significant differences between 24 h and 48 h of incubation.

Although fluorescent probes were not used in the study to mark intracellular structures in order to avoid interference between the bright multicolored fluorescence of the nanocomposite and the marker signal, it is possible to observe a distinct dark region within the cells that, when comparing the fluorescence signal with that of the bright-field images, could be attributed to the nucleus. This observation indicates a negligible nuclear localization of the nanoparticles, with a predominant distribution within the cytosol and organelles. Despite the fact that fluorescence microscopy confirms nanoparticle internalization, precise cytoplasmic localization has not been quantitatively assessed, and future studies employing co-localization with lysosomal or endosomal markers could provide more detailed insights into intracellular trafficking. Based on these findings, it can also be asserted that the nanoparticle composition in terms of percentage of CDs did not influence cellular uptake, which remained similar across all tested samples.

The impact of PCL-CDs NPs on cell viability after internalization was assessed by MTS assay after 48 h of incubation. The results, shown in Fig. 6, highlight the complete cytocompatibility of plain PCL-CDs NPs at all the tested concentrations, with maximum reduction of cell viability to 75 % for PCL-CDs(0.25 %), 82 % for PCL-CDs(0.5 %), and 69 % for PCL-CDs(0.7 %).

Conversely, PCL-CD@DTX demonstrated a dose-dependent cytotoxic effect, albeit with a mitigated impact compared to the free drug. The half-maximal effective concentration (EC_{50}) calculated for the free drug after 48 h (7.61 μg mL^{-1}) is consistent with values reported in the literature, as DTX is known to be particularly effective in inducing breast cancer cell death at low concentrations, making it one of the most promising drugs for the treatment of the most aggressive forms of this cancer, such as the triple-negative subtype. As reported in Table 3, PCL-CDs@DTX exhibited significantly higher EC_{50} values, which may apparently suggest a lower efficacy. However, considering the prolonged drug release profile of the developed nanosystem, the amount actually available to perform the pharmacological action after 48 h is considerably lower than the total amount loaded into the nanosystem (<10 %). Nonetheless, PCL-CDs(0.7 %)@DTX and PCL-CDs(0.25 %) were able to reduce the viability of MDA-MB-231 cells to below 50 % within the tested concentration range, whereas PCL-CDs(0.5 %) led to a reduction of cell viability up to 51.9 % at the highest concentration tested. Therefore, even though the fraction of *in vitro* drug released was small, it was sufficient to induce a marked cytotoxic effect, confirming the effectiveness of the nanosystem in enhancing the antitumor activity of DTX. In addition, this suggests the involvement of alternative release mechanisms inside cells, due to the presence of complex media containing enzymes (e.g., esterases) and ions (i.e. Cu^{+2}, Zn^{+2}, Mn^{+2}, etc.) that can catalyze the bioerosion of the PCL matrix.

3.5. *Storage stability of PCL-CDs NPs and PCL-CDs@DTX in aqueous dispersion*

The storage stability of the PCL-CDs@DTX formulation under dispersion is essential for evaluating its technological transfer and potential application as a drug delivery system in the pharmaceutical market. The colloidal stability of PCL-CDs NPs and PCL-CDs@DTX as aqueous dispersions was evaluated at 25 °C by DLS analysis over time. As reported in Fig. 7, the Z-average of the water-suspended nanoparticles remained almost constant during the analysis time (10 days), indicating that the formulation was not subjected to any instability

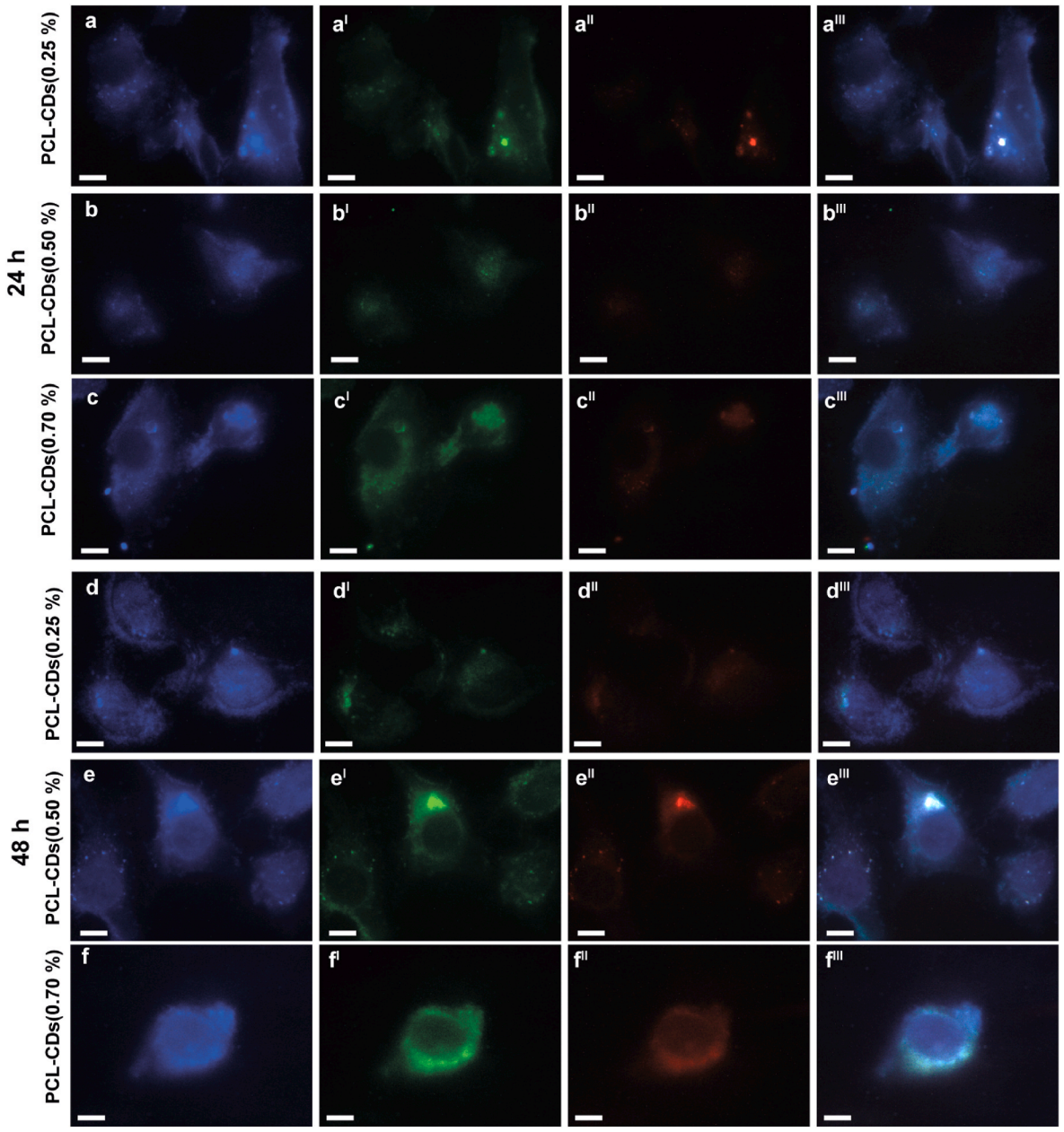

Fig. 5. Cellular uptake of PCL-CDs NPs. Micrographs of MDA-MB-231 cells after 24 h (a–c) or 48 h (d–f) incubation with PCL-CDs(0.25 %) NPs, PCL-CDs(0.5 %) NPs, PCL-CDs(0.7 %) NPs, obtained in the DAPI (a–f), FITC (a'-f'), TxR channel (a''-f''), and merge (a'''-f'''). Scalebar: 10 μm.

phenomenon.

However, in view of the technological transfer to the real-world market, it is preferable to obtain the nanosystem as a dry powder, which is easier to store and requires fewer precautions than its formulation as an aqueous dispersion. However, the freeze-drying of polymeric nanoparticles such as PCL-CDs@DTX can cause irreversible destabilization of the NPs due to their aggregation at the solid state [36]. Cryoprotectants added to the formulation before the freezing should avoid aggregation phenomena by interacting with NPs surfaces and physically interposing between NPs. Even though the cryoprotectant plays a crucial role in preserving the structural and functional characteristics of nanoparticles, including their size and dispersity, which are critical for their biodistribution in biological systems, it does not typically exert specific effects at the biological/nanoparticle interface after the administration. This is because they prevent particle aggregation and freeze damage by displacing the surrounding water and forming a protective amorphous matrix around the nanoparticles; once reconstituted, the cryoprotectant will solubilize and diffuse in the physiological media.

Here, low-molecular-weight poly (ethylene glycol) (PEG 4 kDa), mannitol, and L-arginine were tested as potential cryoprotectants to prevent the destabilization of PCL-CDs@DTX. These compounds have been widely used as colloidal stabilizers during the lyophilization process [37]. Due to their different chemical and physical properties, the selected compounds enable exploring different colloidal stabilization strategies. In detail, the hydroxyl functional group of PEG 4 kDa and mannitol should interact with NPs, forming hydrogen bonds, thus substituting the water molecules and providing steric interference that impairs the intimate contact among NPs; moreover, alcohol sugars like mannitol form a glassy matrix during freezing that embeds NPs, preventing their aggregation [38]. In addition to forming hydrogen bonds with nanoparticles, L-arginine can interact with their surface electrostatically, providing further stabilization [39]. Cryoprotectants were added to the aqueous dispersions of the NPs prior to lyophilization, and

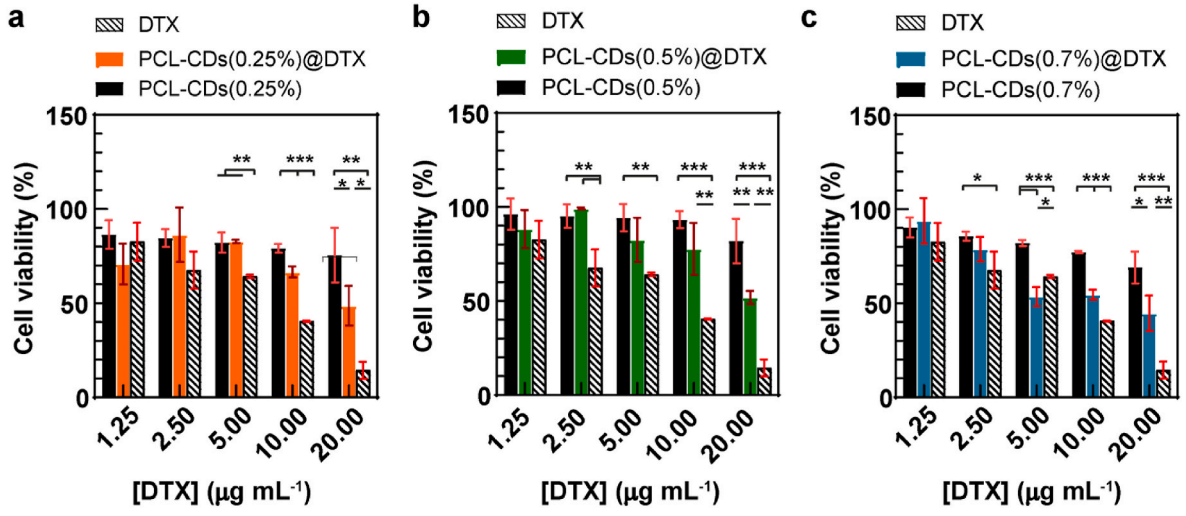

Fig. 6. Cytotoxic effect of PCL-CDs@DTX NPs compared to free docetaxel and plain PCL-CDs NPs. Cell viability of MDA-MB-231 cells after 48 h incubation with PCL-CDs(0.25 %)@DTX NPs (orange) compared to free DTX and plain PCL-CDs(0.25 %) NPs (a), with PCL-CDs(0.5 %)@DTX NPs (green) compared to free DTX and plain PCL-CDs(0.5 %) NPs (b), and with PCL-CDs(0.7 %)@DTX NPs (blue) compared to free DTX and plain PCL-CDs(0.5 %) NPs (c). Data are reported as mean value ± SD (N = 3–5). (For interpretation of the references to color in this figure legend, the reader is referred to the Web version of this article.)

Table 3
Half-maximal efficient concentration (EC_{50}) of PCL-CDs(0.7 %)@DTX, PCL-CDs (0.5 %)@DTX, PCL-CDs(0.25 %)@DTX, and free DTX.

Sample	$EC_{50}^{48\ h}$ (μg mL^{-1} of NPs)	$EC_{50}^{48\ h}$ (μg mL^{-1} of DTX)
PCL-CDs(0.7 %)@DTX	92.7	13.4
PCL-CDs(0.5 %)@DTX	>120.0	>20.0
PCL-CDs(0.25 %)@DTX	129.0	18.9
DTX	/	7.6

the lyophilized powders were subsequently resuspended in water to verify the maintenance of the colloidal properties of the nanoparticles or to observe any aggregation. Results, reported in Table 4, show how the tested cryoprotectants have diverse efficacy on the stabilization of the three samples of PCL-CDs@DTX with increasing CDs content.

In detail, PEG 4 kDa was effective in preserving the dispersibility of PCL-CDs(0.5 %)@DTX, only causing a modest increase in NPs hydrodynamic diameter and maintaining an optimal PDI, but it was ineffective in preventing the aggregation of the other samples. Similarly, mannitol demonstrated inefficacy as cryoprotectant for PCL-CDs(0.5 %)@DTX and PCL-CDs(0.7 %)@DTX, whereas it showed remarkable cryoprotective activity for PCL-CDs(0.25 %)@DTX, which showed limited Z-average increase with good PDI. L-arginine, instead, mitigated the aggregation of all the tested NPs, emerging as best-performing cryoprotectant. The effectiveness of L-arginine compared to the other tested cryoprotectants is relatable to its ionizable functional groups with a positive neat charge, which may favor its interaction with the surface of negatively charged PCL-CDs@DTX. Nevertheless, this interaction does not appear to involve significant adsorption of L-arginine onto the nanoparticles; if a stable amino acid shell had formed on the nanoparticle surface, a reduction in Z-potential would be expected. Instead, a slight increase was observed (~−50 mV), suggesting enhanced electrostatic repulsion between nanoparticles, which likely accounts for their high colloidal stability in aqueous dispersion even after freeze-drying. This unexpected rise in Z-potential indicates a weak interaction with L-arginine, which cryoprotective effect is most likely

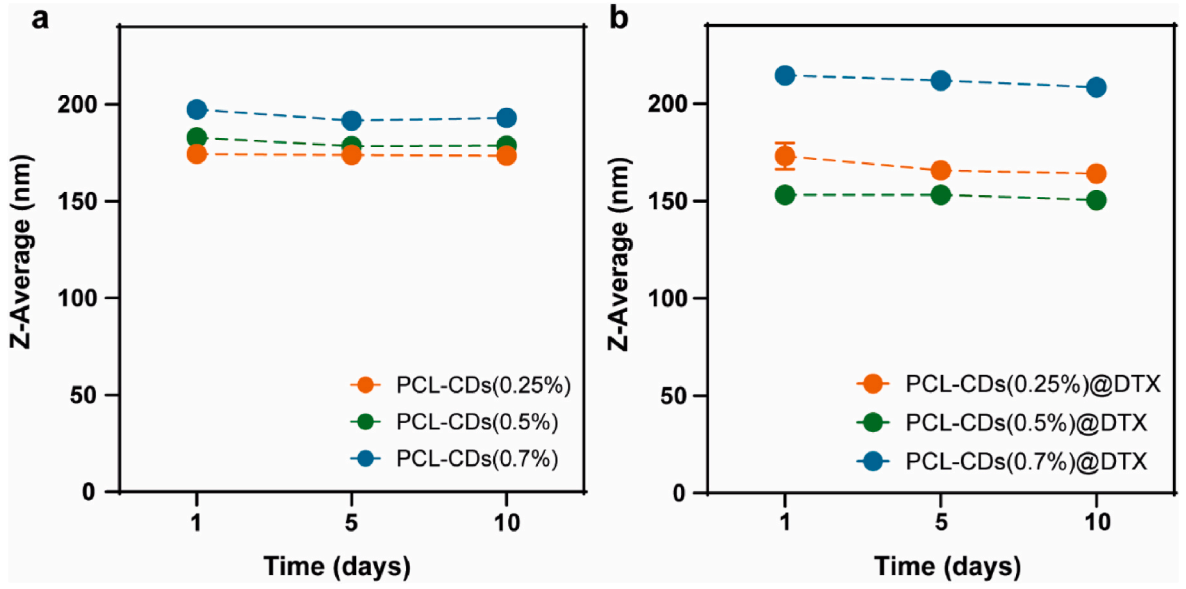

Fig. 7. Colloidal stability of PCL-CDs NPs (a) and PCL-CDs@DTX. Z-average values were obtained by DLS analysis and reported as mean value ± SD (N = 3).

Table 4
Properties of PCL-CDs@DTX in the presence of cryoprotectants.

Nanosystem		BEFORE FREEZE-DRYING			AFTER FREEZE-DRYING		
	Cryoprotectant	**Z-Average (nm)** [a]	**PDI**	**Z-Potential (mV)**	**Z-Average (nm)** [a]	**PDI**	**Z-Potential (mV)** [a]
PCL-CDs(0.25 %)@DTX	PEG 4 kDa	246.3	0.14	−33.0 ± 0.6	Agg.	Agg.	Agg.
PCL-CDs(0.25 %)@DTX	Mannitol	184.3	0.06	−41.1 ± 2.4	202.4	0.06	−22.3 ± 0.6
PCL-CDs(0.25 %)@DTX	L-arginine	180.7	0.01	−48.5 ± 0.8	273.9	0.32	−52.0 ± 0.8
PCL-CDs(0.5 %)@DTX	PEG 4 kDa	175.4	0.07	−47.3 ± 1.7	Agg.	Agg.	Agg.
PCL-CDs(0.5 %)@DTX	Mannitol	167.3	0.01	−39.8 ± 0.1	Agg.	Agg.	Agg.
PCL-CDs(0.5 %)@DTX	L-arginine	175.8	0.04	−54.6 ± 0.5	283.1	0.39	−52.2 ± 1.1
PCL-CDs(0.7 %)@DTX	PEG 4 kDa	233.0	0.07	−46.2 ± 0.7	Agg.	Agg.	Agg.
PCL-CDs(0.7 %)@DTX	Mannitol	229.2	0.01	−38.6 ± 0.3	Agg.	Agg.	Agg.
PCL-CDs(0.7 %)@DTX	L-arginine	189.8	0.01	−49.7 ± 0.6	290.9	0.29	−51.7 ± 0.6

Z-average, PDI, and Z-potential of PCL-CDs@DTX in the presence of cryoprotectants before and after freeze-drying.
[a] Conductivity lower than 1 mS cm^{-1}

attributable to steric hindrance preventing interparticle contact.

4. Conclusions

We successfully developed polycaprolactone-carbon nanodots composite materials, that is PCL–CDs, which combines in the solid state the intrinsic multicolor fluorescence of CDs with the biodegradability and drug delivery capability of PCL. This was achieved by simply adopting an industrially scalable melt-mixing procedure under mild conditions and without using solvents or reactive compounds. Under these conditions, CDs were partially dispersed throughout the polymer matrix conferring self-tracking capability by strong multicolor fluorescence emissions still in solid state.

The hybrid blends were utilized to optimize docetaxel-loaded nanoparticles via nanoprecipitation, using acetone as a green solvent. The resulting formulation exhibited high drug loading (~16.5 %) and excellent encapsulation efficiency (~98 %), along with a uniform particle size distribution (~200 nm) suitable for passive targeting of solid tumors. The rational design of the hybrid nanoparticles resulted in a prolonged and pH-responsive drug release profile. The intrinsic fluorescence of the PCL-CD nanoparticles enabled real-time monitoring of their cellular internalization *in vitro* using a triple-negative breast cancer model. Fluorescence imaging confirmed their efficient uptake by MDA-MB-231 cells and widespread distribution throughout the intracellular compartments, although they did not penetrate the nuclei. Plain PCL–CDs nanoparticles exhibited excellent cytocompatibility, confirming their safety as nanocarriers. After docetaxel encapsulation, PCL–CDs@DTX nanoparticles induced a cytotoxic effect in a dose-dependent manner. The formulation also demonstrated high colloidal stability in aqueous medium up to 10 days, suggesting a suitable shelf-life after dispersion. Moreover, optimization of freeze-drying conditions identified L-arginine as the most effective cryoprotectant, preventing aggregation and ensuring nanoparticle stability after rehydration. Overall, PCL-CDs based nanoparticles demonstrated valuable properties to serve as multifunctional nanoparticles for cancer treatment, enabling efficient and controlled delivery of hydrophobic drugs, as DTX, while ensuring self-trackability by fluorescence imaging.

CRediT authorship contribution statement

Roberta Cillari: Writing – review & editing, Writing – original draft, Validation, Software, Methodology, Investigation, Formal analysis, Data curation. **Francesca Terracina:** Writing – original draft, Methodology, Investigation, Formal analysis, Data curation. **Sergio Sciré:** Writing – review & editing, Methodology, Investigation, Formal analysis, Data curation. **Nicolò Mauro:** Writing – review & editing, Supervision, Resources, Investigation, Funding acquisition, Conceptualization. **Gennara Cavallaro:** Writing – review & editing, Resources, Funding acquisition.

Funding

This research was founded by Fondazione Veronesi by supporting R. C. under the supervision of N.M.

This research was also founded by the European Union - NextGenerationEU through the Italian Ministry of University and Research under PNRR - M4C2-I1.3 Project PE_00000019 ″HEAL ITALIA" to G.C., N.M. and F.T., CUP B73C22001250006 (University of Palermo). The views and opinions expressed are those of the authors only and do not necessarily reflect those of the European Union or the European Commission. Neither the European Union nor the European Commission can be held responsible for them.

S.S. was supported by SiciliAn MicronanOTecH Research And Innovation CEnter "SAMOTHRACE" (MUR, PNRR-M4C2, ECS_00000022), spoke 3 - Universita ' degli Studi di Palermo S2-COMMs - Micro and Nanotechnologies for Smart & Sustainable Communities, for funding.

Declaration of competing interest

The authors declare that they have no known competing financial interests or personal relationships that could have appeared to influence the work reported in this paper.

Acknowledgments

R.C. and N.M. thank Fondazione Veronesi for the FUV Fellowship 2025.

The authors thank ATeN Center – Advanced Technologies Network Center – for the STEM facility.

Data availability

The original contributions presented in this study are included in the article/supplementary material. Further inquiries can be directed to the corresponding authors.

References

[1] Y. Wang, A. Hu, Carbon Quantum Dots: Synthesis, Properties and Applications, 2014, https://doi.org/10.1039/c4tc00988f.
[2] N.A.A. Nazri, N.H. Azeman, Y. Luo, A.A. A Bakar, Carbon quantum dots for optical sensor applications: a review, Opt. Laser Technol. 139 (2021) 106928, https://doi.org/10.1016/J.OPTLASTEC.2021.106928.
[3] K. Hola, Y. Zhang, Y. Wang, E.P. Giannelis, R. Zboril, A.L. Rogach, Carbon dots - emerging light emitters for bioimaging, cancer therapy and optoelectronics, Nano Today 9 (2014) 590–603.
[4] A. Sciortino, A. Cannizzo, F. Messina, Carbon Nanodots: a Review-From the Current Understanding of the Fundamental Photophysics to the Full Control of the Optical Response, 2018, https://doi.org/10.3390/c4040067.
[5] I. Domingues, J. Amaral, B. Vieira, A.L.L. Machado, C.I.M. Santos, J.P.M. Sousa, A. Sciortino, R. Cillari, R. Popescu, Y. Eggeler, et al., Carbon Dots as Dual-Action Nanotools for Detecting and Mitigating Metal Toxicity, 2025, https://doi.org/10.2139/SSRN.5216277.

[6] W. Su, H. Wu, H. Xu, Y. Zhang, Y. Li, X. Li, L. Fan, Carbon dots: a booming material for biomedical applications, Mater. Chem. Front. 4 (2020) 821–836, https://doi.org/10.1039/C9QM00658C.
[7] S. Anwar, H. Ding, M. Xu, X. Hu, Z. Li, J. Wang, L. Liu, L. Jiang, D. Wang, C. Dong, et al., Recent advances in synthesis, optical properties, and biomedical applications of carbon dots, ACS Appl. Bio Mater. 2 (2019) 2317–2338, https://doi.org/10.1021/ACSABM.9B00112/ASSET/IMAGES/LARGE/MT-2019-001123_0012.JPEG.
[8] I. Domingues, J. Amaral, B. Vieira, A.L. Machado, C.I.M. Santos, J.P.M. Sousa, A. Sciortino, R. Cillari, R. Popescu, Y.M. Eggeler, et al., Carbon dots as dual-action nanotools for metal toxicity recognition and mitigation, Environ. Res. 286 (2025) 122851, https://doi.org/10.1016/J.ENVRES.2025.122851.
[9] Z. Feng, K.H. Adolfsson, Y. Xu, H. Fang, M. Hakkarainen, M. Wu, Carbon dot/polymer nanocomposites: from green synthesis to energy, environmental and biomedical applications, Sustain. Mater. Technol. 29 (2021) e00304, https://doi.org/10.1016/J.SUSMAT.2021.E00304.
[10] J. Chen, X. Guo, R. Tan, M. Huang, J. Ren, W. Liu, M. Wang, B. Li, Z. Ma, Q. Zhang, Achieving the simultaneous improvement of degradation, thermal, and mechanical properties of polylactic acid composite films by carbon quantum dots, Compos. B Eng. 299 (2025) 112442, https://doi.org/10.1016/J.COMPOSITESB.2025.112442.
[11] N. Mauro, M. Andrea Utzeri, A. Sciortino, M. Cannas, F. Messina, G. Cavallaro, G. Giammona, Printable Thermo- and photo-stable Poly(D,L-Lactide)/Carbon nanodots nanocomposites via heterophase melt-extrusion transesterification, Chem. Eng. J. 443 (2022) 136525, https://doi.org/10.1016/J.CEJ.2022.136525.
[12] N. Mauro, G. Calabrese, A. Sciortino, M.G. Rizzo, F. Messina, G. Giammona, G. Cavallaro, Microporous fluorescent Poly(D,L-Lactide) acid–carbon nanodot scaffolds for bone tissue engineering applications, Materials 17 (2024), https://doi.org/10.3390/ma17020449.
[13] P.F. Rossi, F.V. dos Santos, A.L.M.M. Alves, L.H. Semensato, L.F.R. Oliveira, D. M. dos Santos, T. de Paula Bianchi, N.M. Inada, S.P. Campana-Filho, R.L. Oréfice, et al., 3D-Printed methacrylated gelatin-lignin carbon dot hydrogel combined with PLA nanofibers for wound dressings, ACS Appl. Nano Mater. (2024), https://doi.org/10.1021/ACSANM.4C03615/ASSET/IMAGES/LARGE/AN4C03615_0006.JPEG.
[14] R. Cillari, A. Sciortino, S. Scire, M. Cannas, F. Messina, N. Mauro, Fluorescence switching in PH-Responsive Poly(Amidoamine) hydrogel networks containing gold nanoparticles and carbon nanodots for potential real-time tumor PH monitoring, ACS Applied Optical Materials (2025), https://doi.org/10.1021/ACSAOM.5C00194.
[15] R. Pathak, V.D. Punetha, S. Bhatt, M. Punetha, Multifunctional role of carbon dot-based polymer nanocomposites in biomedical applications: a review, J. Mater. Sci. 58 (2023) 6419–6443, https://doi.org/10.1007/S10853-023-08408-4/METRICS.
[16] I. Armentano, M. Gigli, F. Morena, C. Argentati, L. Torre, S. Martino, Recent advances in nanocomposites based on aliphatic polyesters: design, synthesis, and applications in regenerative medicine, Appl. Sci. 8 (2018), https://doi.org/10.3390/APP8091452. *Page 1452* **2018**, *8*, 1452.
[17] L.N. Woodard, M.A. Grunlan, Hydrolytic degradation and erosion of polyester biomaterials, ACS Macro Lett. 7 (2018) 976, https://doi.org/10.1021/ACSMACROLETT.8B00424.
[18] S. Slomkowski, T. Basinska, M. Gadzinowski, D. Mickiewicz, Polyesters and polyester Nano- and microcarriers for drug delivery, Polymers 16 (2024) 2503, https://doi.org/10.3390/POLYM16172503. Page 2503 2024, 16.
[19] F. Mohamed, C.F. Van Der Walle, Engineering biodegradable polyester particles with specific drug targeting and drug release properties, J. Pharmacol. Sci. 97 (2008) 71–87, https://doi.org/10.1002/JPS.21082.
[20] D. Mondal, M. Griffith, S.S. Venkatraman, Polycaprolactone-based biomaterials for tissue engineering and drug delivery: current scenario and challenges, Int. J. Polym. Mater. Polym. Biomater. 65 (2016) 255–265, https://doi.org/10.1080/00914037.2015.1103241.
[21] T.K. Dash, V.B. Konkimalla, Poly-ε-Caprolactone based formulations for drug delivery and tissue engineering: a review, J. Contr. Release 158 (2012) 15–33, https://doi.org/10.1016/J.JCONREL.2011.09.064.
[22] H. He, Y. Xie, Y. Lv, J. Qi, X. Dong, W. Zhao, W. Wu, Y. Lu, Bioimaging of intact polycaprolactone nanoparticles using aggregation-caused quenching probes: size-dependent translocation via oral delivery, Adv. Healthcare Mater. 7 (2018) 1800711, https://doi.org/10.1002/ADHM.201800711.
[23] J.P. Abriata, R.C. Turatti, M.T. Luiz, G.L. Raspantini, L.B. Tofani, R.L.F. do Amaral, K. Swiech, P.D. Marcato, J.M. Development Marchetti, Characterization and biological in vitro assays of paclitaxel-loaded PCL polymeric nanoparticles, Mater. Sci. Eng. C 96 (2019) 347–355, https://doi.org/10.1016/J.MSEC.2018.11.035.
[24] S.C. Ray, A. Saha, N.R. Jana, R. Sarkar, Fluorescent carbon nanoparticles: synthesis, characterization, and bioimaging application, J. Phys. Chem. C 113 (2009) 18546–18551, https://doi.org/10.1021/jp905912n.
[25] S.T. Yang, X. Wang, H. Wang, F. Lu, P.G. Luo, L. Cao, M.J. Meziani, J.H. Liu, Y. Liu, M. Chen, et al., Carbon dots as nontoxic and high-performance fluorescence imaging agents, J. Phys. Chem. C 113 (2009) 18110–18114, https://doi.org/10.1021/jp9085969.
[26] N. Mauro, M.A. Utzeri, A. Sciortino, F. Messina, M. Cannas, R. Popescu, D. Gerthsen, G. Buscarino, G. Cavallaro, G. Giammona, Decagram-scale synthesis of multicolor carbon nanodots: self-tracking nanoheaters with inherent and selective anticancer properties, ACS Appl. Mater. Interfaces 14 (2022) 2551–2563, https://doi.org/10.1021/ACSAMI.1C19599/ASSET/IMAGES/LARGE/AM1C19599_0006.JPEG.
[27] N.J. Simi, S. Bharathi Bernadsha, Green chemistry approaches for sustainable synthesis of polymeric nanomaterials, Nanotechnol. Plant Sci. 2 (2025) 311–337, https://doi.org/10.1007/978-3-031-84643-4_11.
[28] V. Torchilin, Tumor delivery of macromolecular drugs based on the EPR effect, Adv. Drug Deliv. Rev. 63 (2011) 131–135, https://doi.org/10.1016/J.ADDR.2010.03.011.
[29] H. Kang, S. Rho, W.R. Stiles, S. Hu, Y. Baek, D.W. Hwang, S. Kashiwagi, M.S. Kim, H.S. Choi, Size-dependent EPR effect of polymeric nanoparticles on tumor targeting, Adv. Healthcare Mater. 9 (2020) e1901223, https://doi.org/10.1002/ADHM.201901223.
[30] D.J. Pochapski, C. Carvalho Dos Santos, G.W. Leite, S.H. Pulcinelli, C.V. Santilli, Zeta potential and colloidal stability predictions for inorganic nanoparticle dispersions: effects of experimental conditions and electrokinetic models on the interpretation of results, Langmuir 37 (2021) 13379–13389, https://doi.org/10.1021/ACS.LANGMUIR.1C02056.
[31] D. Zhu, W. Tao, H. Zhang, G. Liu, T. Wang, L. Zhang, X. Zeng, L. Mei, Docetaxel (DTX)-loaded polydopamine-modified TPGS-PLA nanoparticles as a targeted drug delivery system for the treatment of liver cancer, Acta Biomater. 30 (2016) 144–154, https://doi.org/10.1016/J.ACTBIO.2015.11.031.
[32] X. Wang, Y. Gu, Q. Li, Y. Xu, Y. Shi, Z. Wang, M. Xia, J. Li, D. Wang, Synergistic chemo-photothermal cancer therapy of PH-Responsive polymeric nanoparticles loaded IR825 and DTX with charge-reversal property, Colloids Surf. B Biointerfaces 209 (2022) 112164, https://doi.org/10.1016/J.COLSURFB.2021.112164.
[33] C.K. Phillips, D.P. Docetaxel Petrylak, Drug Management of Prostate Cancer, 2024, pp. 133–146, https://doi.org/10.1007/978-1-60327-829-4_12.
[34] J.M. White, J. Jurczyk, R.M. Van Horn, Physical structure contributions in PH degradation of PEO-b-PCL films, Polym. Degrad. Stabil. 183 (2021) 109468, https://doi.org/10.1016/J.POLYMDEGRADSTAB.2020.109468.
[35] S. Manchun, C.R. Dass, P. Sriamornsak, Targeted therapy for cancer using PH-Responsive nanocarrier systems, Life Sci. 90 (2012) 381–387, https://doi.org/10.1016/J.LFS.2012.01.008.
[36] W.C. Luo, A. O'Reilly Beringhs, R. Kim, W. Zhang, S.M. Patel, R.H. Bogner, X. Lu, Impact of formulation on the quality and stability of freeze-dried nanoparticles, Eur. J. Pharm. Biopharm. 169 (2021) 256–267, https://doi.org/10.1016/J.EJPB.2021.10.014.
[37] P. Fonte, S. Reis, B. Sarmento, Facts and evidences on the lyophilization of polymeric nanoparticles for drug delivery, J. Contr. Release 225 (2016) 75–86, https://doi.org/10.1016/J.JCONREL.2016.01.034.
[38] W. Abdelwahed, G. Degobert, S. Stainmesse, H. Fessi, Freeze-drying of nanoparticles: formulation, process and storage considerations, Adv. Drug Deliv. Rev. 58 (2006) 1688–1713, https://doi.org/10.1016/J.ADDR.2006.09.017.
[39] P. Stärtzel, Arginine as an excipient for protein freeze-drying: a mini review, J. Pharmacol. Sci. 107 (2018) 960–967, https://doi.org/10.1016/J.XPHS.2017.11.015.